

# A calculation of the QCD phase diagram at finite temperature, and baryon and isospin chemical potentials

A. Barducci, R. Casalbuoni, G. Pettini, L. Ravagli

*Department of Physics, University of Florence and INFN Sezione di Firenze*

*Via G. Sansone 1, I-50109, Sesto F.no, Firenze, Italy\**

We study the phases of a two-flavor Nambu-Jona-Lasinio model at finite temperature  $T$ , baryon and isospin chemical potentials:  $\mu_B = (\mu_u + \mu_d)/2$ ,  $\mu_I = (\mu_u - \mu_d)/2$ . This study completes a previous analysis where only small isospin chemical potentials  $\mu_I$  were considered.

PACS numbers: 11.10.Wx, 12.38.-t, 25.75.Nq

## I. INTRODUCTION

The possible formation of a pion condensate due to a finite isospin chemical potential  $\mu_I$  has been, in recent years, the subject of several papers [1, 2, 3, 4, 5, 6, 7, 8, 9, 10, 11, 12, 13, 14]. Consequently, the reconstruction of the QCD phase diagram at finite temperature and quark densities, such as those attainable in earth experiments and in the interior of stars, is even more challenging due to the addition of  $\mu_I$ , besides temperature  $T$  and baryon chemical potential  $\mu_B$ . Various regions of the phase diagram correspond to different experimental settings. Actually, the behavior of QCD at high temperature and low baryon densities is central to the relativistic heavy-ion collisions: experiments at CERN and RHIC are expected to produce hadronic matter in this regime. On the other hand, the description of neutron star interiors requires the knowledge of cold nuclear matter at large baryon densities. However, nature does also provide us with systems at finite isospin chemical potential  $\mu_I$  in the form of asymmetric-isospin matter inside neutron stars: nuclear matter has a finite (negative) isospin  $I_3$  density due to Coulomb interactions, apart from finite baryon-number density. Moreover, in any realistic experimental setting in relativistic heavy-ion collisions

---

\*Electronic address: barducci@fi.infn.it, casalbuoni@fi.infn.it, pettini@fi.infn.it, ravagli@fi.infn.it

there is a non-zero, even if small,  $\mu_I$ .

Our present description of the QCD phase diagram in the plane  $(\mu_B, T)$  anticipates the existence of a tricritical point separating first order transitions in the regions of low temperatures from cross-over transitions in the low baryon chemical potential and high temperature regime [15, 16, 17, 18, 19, 20, 21]. In recent years various other non-trivial phases of QCD at low temperatures and high baryon chemical potentials have been discovered, such as the Color Flavor Locking (CFL) phase and the two-color superconducting (2SC) phase (for a review see [22]).

Coming back to the effects of the isospin chemical potential  $\mu_I$ , pion condensation has so far been primarily investigated by means of low energy models based on chiral lagrangians [5, 7, 8, 23]. Although these models are well suited to study the phases of QCD as they have the right symmetry properties, they do not include the combined effects of the isospin chemical potential  $\mu_I$  with a finite baryon chemical potential  $\mu_B$  in order to study the pattern of chiral symmetry breaking and restoration as well. To consider both  $\mu_B$  and  $\mu_I$ , we need a model with quarks as microscopic degrees of freedom. The effect of small  $\mu_I$  (up to half of the pion mass) has been investigated in ref. [12] in the context of the Nambu-Jona-Lasinio model and in *ladder*-QCD [14]. The result is the splitting of the critical curves for chiral symmetry restoration for the two light flavors, whereas a full study for arbitrary  $\mu_I$  has only been done in the context of a random matrix model [11].

Studies on the lattice have been performed at finite  $\mu_I$  and  $\mu_B = 0$  in refs. [24, 25, 26, 27, 28] and with a finite  $\mu_B$  and  $\mu_I = 0$  in refs. [28, 29, 30, 31, 32]. In a recent work [33] the effect of both  $\mu_B$  and a small  $\mu_I$  has also been considered. The case of high  $\mu_B$  and small  $\mu_I$  has been considered in [34].

In this work we extend the analysis of [12, 14] where it was found that the first order transition line ending at the tricritical point of the case  $\mu_I = 0$  actually splits into two first order transition lines and correspondingly two crossover regions are present at low values of baryon chemical potential. In particular we will be working in the context of a NJL model with a form factor included such as to imply a decreasing of the fermion self-energy compatible with the operator product expansion.

It should also be noticed that in [13] the NJL model has been augmented by the four-fermi instanton interaction relevant in the case of two flavors. These authors have found that the coupling induced by the instanton interaction between the two flavors might completely

wash the splitting of the first order transition line. This happens for values of the ratio of the instanton coupling to the NJL coupling of order 0.1-0.15.

In Section II we summarize the relevant features of the NJL model we have considered, with isospin charge included. The one-loop effective potential and the values of the fit parameters are included. In Section III we discuss the various equilibrium phases of the model, together with the corresponding symmetries, by studying the behavior of the scalar and pion condensates with respect to different thermodynamical parameters among  $T, \mu_B, \mu_I$  (or  $\mu_u, \mu_d$ ). Results are shown for growing temperatures, starting from zero up to temperatures above that of the critical ending point. Finally, Section IV is devoted to conclusions.

## II. THE MODEL

Our purpose is to explore the structure of the phase diagram for chiral symmetry and pion condensation in QCD at finite temperature and quark densities, by using a microscopic model with quark degrees of freedom. This task has been accomplished, up to now, in the context of a random matrix model simulating QCD with two flavors [11] and, in the case of small differences between the  $u$  and  $d$  quark chemical potentials, also in the Nambu-Jona-Lasinio model (NJL) [12] and in *ladder*-QCD [14].

One reason for using a model with quarks as microscopic degrees of freedom is that it gives us the possibility of studying chiral symmetry breaking and pion condensation at both finite isospin and baryon chemical potentials, which is not possible within effective chiral models. In ref. [12], the authors made use of the NJL model with a suitable form factor included in the quark self-energy to mimic asymptotic freedom [21, 35]. This version of the NJL model turns out to be very close to *ladder*-QCD as developed in refs. [16, 36] where the momentum dependence of the quark self-energy is consistently dictated by the study of the Schwinger-Dyson equation within a variational approach (see the previous references for details). However, although *ladder*-QCD is a covariant and self-consistent approach, the dependence on the four-momentum of the quark self-energy makes the numerical computation of the one-loop effective potential with finite quark densities much more onerous with respect to the NJL case, where the quark self-energies depend only on the three-momentum. For this reason, in the present work we study the NJL model. It is reasonable to expect that when employing *ladder*-QCD, the resulting physical picture does not considerably differ

from that of the NJL model. This has been the case in previous applications too [16, 17, 19].

As already said in the Introduction we are not going to consider the effects of di-fermion condensation. Therefore our results can be considered valid only outside the region of the color superconductive phase, which is roughly in the region defined by  $\mu_B \gtrsim 400 - 500 \text{ MeV}$  and  $T \lesssim 50 \text{ MeV}$ . At the same time we will not consider regions at values of  $\mu_u$  or  $\mu_d$  higher than  $400 - 500 \text{ MeV}$  where other difermion condensates might arise (see for instance ref. [37]).

Let us now consider the Lagrangian of the NJL model with two flavors  $u, d$  with the same mass  $m$  but different chemical potentials  $\mu_u$  and  $\mu_d$

$$\begin{aligned} \mathcal{L} &= \mathcal{L}_0 + \mathcal{L}_m + \mathcal{L}_\mu + \mathcal{L}_{int} \\ &= \bar{\Psi} i \hat{\partial} \Psi - m \bar{\Psi} \Psi + \Psi^\dagger A \Psi + \frac{G}{2} \sum_{a=0}^3 \left[ (\bar{\Psi} \tau_a \Psi)^2 + (\bar{\Psi} i \gamma_5 \tau_a \Psi)^2 \right] \end{aligned} \quad (1)$$

where  $\Psi = \begin{pmatrix} u \\ d \end{pmatrix}$ ,  $A = \begin{pmatrix} \mu_u & 0 \\ 0 & \mu_d \end{pmatrix}$  is the matrix of chemical potentials and  $\tau_a$ ,  $a = 0, 1, 2, 3$ , is the set of the three Pauli matrices plus the identity.

We note that we can express  $\mathcal{L}_\mu$  either by using the variables  $\mu_u, \mu_d$  or the two combinations  $\mu_B = \frac{\mu_u + \mu_d}{2}$  and  $\mu_I = \frac{\mu_u - \mu_d}{2}$ , which couple to the baryon charge density and to the third component of isospin respectively

$$\mathcal{L}_\mu = \mu_B \Psi^\dagger \Psi + \mu_I \Psi^\dagger \tau_3 \Psi \quad (2)$$

To study whether a pion condensate shows up, we need to calculate the effective potential. This is obtained by using the standard technique to introduce bosonic (collective) variables through the Hubbard-Stratonovich transformation and by integrating out the fermion fields in the generating functional. However, the effective potential that we have considered is not directly obtained from the Lagrangian in Eq. (1). To mimic asymptotic freedom we want to include a form factor as in ref. [35] and we thus follow the same procedure as in refs. [12, 21]. The result is a one-loop effective potential which generalizes that of the theory described by the Lagrangian in Eq. (1), and which reduces to it in the limit of a constant form factor  $F(\vec{p}) = 1$ .

$$V = \frac{\Lambda^2}{8G} (\chi_u^2 + \chi_d^2 + 2\rho^2) + V_{\log} \quad (3)$$

$$V_{\log} = -\text{Tr} \log \begin{pmatrix} h_u & -F^2(\vec{p}) \Lambda \rho \gamma_5 \\ F^2(\vec{p}) \Lambda \rho \gamma_5 & h_d \end{pmatrix} \quad (4)$$

$$h_f = (i\omega_n + \mu_f)\gamma_0 - \vec{p} \cdot \vec{\gamma} - (m + F^2(\vec{p}) \Lambda \chi_f)$$

where  $\omega_n$  are the Matsubara frequencies and the dimensionless fields  $\chi_f$  and  $\rho$  are connected to the condensates by the following relations

$$\begin{aligned} \chi_f &= -2G \frac{\langle \bar{\Psi}_f \Psi_f \rangle}{\Lambda} \\ \rho &= -G \frac{\langle \bar{u} \gamma_5 d - \bar{d} \gamma_5 u \rangle}{\Lambda} \end{aligned} \quad (5)$$

and are variationally determined at the absolute minimum of the effective potential. In the previous equations,  $\Lambda$  is a mass scale appearing in the form factor  $F(\mathbf{p}^2) = \frac{\Lambda^2}{\Lambda^2 + \mathbf{p}^2}$  [35]. It is worth noting that the one-loop effective potential in Eq. (4) has the same expression of the one derived in ref. [14] within *ladder*-QCD. Therein, multiplying the scalar and pseudoscalar fields, there was a test function guessed from the study of the one-loop Schwinger-Dyson equation for the quark self-energy, in place of  $F^2(\vec{p})$  in Eq. (4). The only difference is that  $F^2$  depends on the three-momentum whereas the quoted test function depends on the four-momentum and that the two asymptotic behaviors are different ( $\sim 1/p^2$  in the test function of ref. [14] and  $\sim 1/\vec{p}^4$  in  $F^2$  of Eq. (4)). Otherwise the two effective potentials would be identical. This observation also explains the reason why we have adopted the NJL model instead of *ladder*-QCD to generalize the analysis of ref. [14] at high isospin chemical potentials as the numerical analysis is much simpler in this case.

To fix the free parameters of the model, which are  $\Lambda$ , the average current quarks mass  $m = (m_u + m_d)/2$  and the coupling  $G = g/\Lambda^2$ , we work at zero temperature and quark densities. We first choose the mass scale  $\Lambda$  within the range  $\Lambda \sim 500 - 600 \text{ MeV}$ . Then we determine the strength of the coupling  $g$  and the mass parameter  $m$  by requiring a light quark condensate of the order  $\langle \bar{\Psi}_f \Psi_f \rangle \simeq -(200 \text{ MeV})^3$  and a pion mass  $m_\pi \simeq 140 \text{ MeV}$  (the latter evaluated through the curvature of the effective potential in the direction of the pion field and having fixed  $f_\pi$  at its experimental value [36]).

The output parameters are the following

$$\Lambda = 580 \text{ MeV}; \quad g = 7; \quad m = 4.5 \text{ MeV} \quad (6)$$

With these values we obtain a condensate  $\langle \bar{\Psi}_f \Psi_f \rangle = -(172 \text{ MeV})^3$  and a constituent quark mass  $M_f = 428 \text{ MeV}$  (defined as in [19, 21]). The critical isospin chemical potential at zero temperature turns out to be  $\mu_I^C = 89 \text{ MeV}$ . The discrepancy of about 25% (we recall that the expected value of  $\mu_I^C$  would be  $m_\pi/2 \simeq 70 \text{ MeV}$ ) is due to the approximate fit procedure. Actually, in our previous work based on *ladder*-QCD [14], where  $f_\pi$  was consistently calculated within the model, we got  $\mu_I^C = m_\pi/2$ .

### III. PHASE DIAGRAM FOR CHIRAL SYMMETRY BREAKING AND PION CONDENSATION

In order to discuss the structure of the phase diagram, it is worth summarizing the symmetries of the Lagrangian density in Eq. (1). Both  $\mathcal{L}_0$  and  $\mathcal{L}_{int}$  are  $SU_L(2) \otimes SU_R(2) \otimes U_V^B(1) \otimes U_A^B(1)$  invariant. The symmetry is reduced by the mass term  $\mathcal{L}_m$  to  $SU_V(2) \otimes U_V^B(1)$  and further reduced from the term  $\mathcal{L}_\mu$  which selects a direction in the isospin space, as is evident from Eq. (2), unless  $\mu_u = \mu_d$  and thus  $\mu_I = 0$ . The remaining symmetry can be expressed either as  $U_V^u(1) \otimes U_V^d(1)$  or  $U_V^B(1) \otimes U_V^I(1)$ , depending on the basis of the fields that we are choosing.

The baryon number symmetry  $U_V^B(1)$  is dynamically respected, whereas a non vanishing v.e.v. of the  $\rho$  field defined in Eq. (5) may appear, which dynamically breaks  $U_V^I(1)$ . This implies the appearance of a Goldstone mode, which is either the charged  $\pi^+$  or  $\pi^-$  at the threshold, depending on the sign of  $\mu_I$ , whereas the other two pions are massive modes.

As far as the scalar condensates  $\chi_u, \chi_d$  (see Eq. (5)) are concerned, they do not break any symmetry. However, since the mass term is small, their value is almost entirely due to the approximate spontaneous breaking of chiral symmetry. Consequently we distinguish regions where the dynamical effect is relevant, from regions where the scalar condensates are of order  $\sim m/\Lambda$ , namely where only the effect of the explicit breaking of chiral symmetry survives.

The determination of the various phases has been performed numerically by minimizing the one-loop effective potential. We start by showing the results in the  $(\mu_u, \mu_d)$  plane, for fixed

values of the temperature. Different regions are labelled, as in ref. [11], by the symbol of the field which acquires a non vanishing v.e.v. due to dynamical effects, whereas the other fields are vanishing ( $\rho$ ), or of the order  $\sim m/\Lambda$  ( $\chi_u$  and/or  $\chi_d$ ).

Solid lines refer to discontinuous transitions and dashed lines to continuous ones. However, we recall that strictly speaking only the lines surrounding regions with a non vanishing field  $\rho$  refer to genuine phase transitions, associated with the breaking and restoration of the  $U_V^I(1)$  symmetry.

### A. Zero temperature

In Fig. 1 we show the phase diagram in the  $(\mu_u, \mu_d)$  plane at zero temperature. Let us start from the vacuum at  $T = \mu_u = \mu_d = 0$ , at the center of the picture. Here, in the chiral limit, the pions are the Goldstone bosons associated with the spontaneous breaking of  $SU(2)_L \otimes SU(2)_R$ . We have chosen these variables in order to compare the structure of the phase diagram with that obtained in ref. [11]. However, if we want to recover known results given in terms of the baryon chemical potential, we have to move from the center along the diagonal at  $\mu_u = \mu_d$  and thus at  $\mu_I = 0$ , and increase the absolute value of  $\mu_B$ . At  $\frac{|\mu_u + \mu_d|}{2} = |\mu_B| = 293 \text{ MeV}$  we meet the approximate restoration of chiral symmetry due to the sudden jump of the condensates of the two (degenerate) quarks to values of order  $\sim m/\Lambda$ , which is a discontinuous transition. The same thing happens by moving along lines parallel to the main diagonal in the region labelled by  $\chi_u, \chi_d$ , enclosed between the two dashed lines at  $\frac{|\mu_u - \mu_d|}{2} = |\mu_I| = 89 \text{ MeV}$  (see also Fig. 2 where it is shown that the critical value of  $\mu_I$  at  $T = 0$  is independent on  $\mu_B$ ) and by varying  $|\mu_B|$ . The regions in the top-right and bottom-left corners of Fig. 1 thus have the  $U_V^u(1) \otimes U_V^d(1)$  symmetry of  $\mathcal{L}$  with  $\rho = 0$  and  $\chi_u, \chi_d$  of order  $\sim m/\Lambda$ .

By moving from the center along the diagonal at  $\mu_u = -\mu_d$  (and thus  $\mu_B = 0$ ) or parallel to it, when crossing one of the two dashed lines at  $|\mu_I| = 89 \text{ MeV}$  (we have already discussed the origin of the discrepancy between this value and half of the pion mass in the model), the absolute minimum of the effective potential starts to rotate along the  $\rho$  direction. We thus have a continuous breaking of  $U_V^I(1)$  and a second order phase transition with one Goldstone mode which is, right along the dashed line, either the  $\pi^+$  (in the upper part of the diagram) or the  $\pi^-$  (in the lower part). In the chiral limit these two dashed lines merge together

in coincidence with the diagonal at  $\mu_I = 0$  as the pion becomes massless in this limit and the rotation is sudden, giving first order phase transitions for pion condensation. In this case there are two Goldstone bosons associated with the spontaneous breaking of two  $U(1)$  symmetry groups ( $U_A^B(1) \otimes U_V^I(1)$ ) [25].

Coming back to the massive case, and still with reference to Fig. 1, we conclude that by considering  $|\mu_B|$  not too large and by growing  $|\mu_I|$ , we find a second order phase transition with the rotation of the scalar condensates into the pseudoscalar, namely we are faced with pion condensation in a relatively simple picture. A difference with ref. [11] is that we do not find the vanishing of  $\rho$  for values of  $|\mu_I|$  high with respect to the pion mass, but still sufficiently low to avoid considering superconductive phases (actually, for very low  $|\mu_B|$  this transition would occur in the present model for  $|\mu_I| \sim 1 \text{ GeV}$ ).

To explore the possibility of multiple phase transitions and thus of a richer phenomenology, we need to grow  $|\mu_B|$  as for instance we do in the case described in Fig. 3 where we follow the path of the solid line  $a$  in Fig. 1 at  $\mu_B = 170 \text{ MeV}$  for growing  $\mu_I \geq 0$ . The fields  $\chi_u$  and  $\chi_d$  are almost degenerate, both in the region of the approximate dynamical breaking of chiral symmetry (below  $\mu_I = 89 \text{ MeV}$ ) and in the region of spontaneous breaking of  $U_V^I(1)$ , where they rotate into the  $\rho$  field. Then, when the line  $a$  in Fig. 1 crosses the solid line surrounding the region labelled by  $\chi_d$ , we see that  $\rho$  suddenly jumps to zero with the restoration of the  $U_V^I(1)$  group and that  $\chi_u$  and  $\chi_d$  split. Actually the latter suddenly acquires a value due to the dynamical breaking of chiral symmetry whereas  $\chi_u$  undergoes a further decrease and remains of order  $\sim m/\Lambda$ .

In Fig. 4 we plot the behavior of the scalar condensates  $\chi_u$  and  $\chi_d$  vs.  $\mu_I$  at  $\mu_B = 210 \text{ MeV}$ , namely by following the path described by the solid line  $b$  in Fig. 1. We see that we never cross the region with  $\rho \neq 0$  and that we simply pass from a region where the dynamical effect of the breaking of chiral symmetry is entirely due to a large value of  $\chi_u$  and  $\chi_d$  of order  $\sim m/\Lambda$  (at large negative  $\mu_I$  and small  $\mu_u$ ), to a region where this effect manifests itself with a large value of  $\chi_d$  and  $\chi_u$  of order  $\sim m/\Lambda$  (at large positive  $\mu_I$  and small  $\mu_d$ ). The region in between has almost degenerate and both large  $\chi_u$  and  $\chi_d$ . Pion condensation does not occur for this value of  $\mu_B$  (see also Fig. 2).

Finally, in Fig. 5, we plot the behavior of the condensates at fixed  $\mu_u = 200 \text{ MeV}$  vs.  $\mu_d$  (see again Fig. 1). The rotation of the pion condensate into the scalar ones occurs when the vertical line at  $\mu_u = 200 \text{ MeV}$  meets the dashed line at  $\mu_I = 89 \text{ MeV}$ , which happens for



$\mu_d$  of few  $MeV$ . Then, when  $\mu_d$  has sufficiently increased,  $\chi_d$  falls to a small value of order  $\sim m/\Lambda$  with a discontinuous transition, whereas  $\chi_u$  remains constant at its large value.

## B. Finite temperature

The evolution of the phase diagram for growing temperatures is easily understood as far as the regions with  $\rho = 0$  are concerned. Actually, in this case the effective potential at the minimum is the sum of two independent terms, one for each flavor, and the results are straightforwardly given through the analysis of chiral symmetry breaking and restoration for a single flavor at finite temperature and chemical potential (see for instance refs. [16, 18]). In Fig. 6 we show the phase diagram at zero, or small isospin chemical potential (see also refs. [12, 14]). From this picture we see that moving along any of the critical lines of chiral symmetry restoration at fixed  $\mu_I$ , the critical value of the baryon chemical potential  $\mu_B$  decreases for growing temperatures. Furthermore, for temperatures below that of the critical ending point  $E$ ,  $T < T(E) = 85 \text{ MeV}$ , the transitions are always discontinuous whereas they become cross-over transitions for  $T > T(E)$ . Consequently the regions labelled by  $\chi_u$  and/or  $\chi_d$  in Fig. 1 shrink when growing  $T$  and their rectilinear sides become lines of cross-over transitions for  $T > T(E)$  (see Fig. 1 and Figs. 7, 8 where we plot the phase diagrams in the  $(\mu_u, \mu_d)$  plane at  $T = 60 \text{ MeV}$  and  $T = 140 \text{ MeV}$ , which is respectively below and above  $T(E)$ ). The new feature concerns the regions with  $\rho \neq 0$ , which also reduce their size for growing  $T$ , whereas the order of the transitions starts to change from first to second, beginning from the critical points at highest  $|\mu_I|$ , until they reach the points of the boundaries which coincide with those of the regions labelled by  $\chi_u$  or  $\chi_d$  (see Fig. 8). Also the length of the curves of second order phase transitions to pion condensation at fixed values of  $|\mu_B|$  sensibly reduces from low temperatures to high temperatures (see again Fig. 1, and Figs. 7, 8). A similar behavior, for high  $T$ , is found in ref. [11]. For  $T > T(P_T) = 174 \text{ MeV}$ , which is the cross-over temperature at zero chemical potential (see Fig. 6), all these regions disappear from the phase diagram, which is thus characterized by  $\rho = 0$  and  $\chi_u, \chi_d \sim m/\Lambda$ .

The behavior of the scalar and pseudoscalar condensates at  $T = 60 \text{ MeV}$  are much similar to those at  $T = 0$ . As an example we plot, in Fig. 9, the condensates at  $\mu_u = 200 \text{ MeV}$  and  $T = 60 \text{ MeV}$  vs.  $\mu_d$  (compare with Fig. 5). The situation is different if we consider

temperatures above  $T(E) = 85 \text{ MeV}$ . For instance, at  $T = 140 \text{ MeV}$ , we see from Fig. 8, that the structure of the phase diagram is only slightly modified with respect to the case of two independent flavors which undergo cross-over phase transitions at sufficiently high values of their own chemical potentials (actually the region of pion condensation has sensibly reduced with respect to Figs. 1, 7). The phase transition associated with the spontaneous breaking of  $U_V^I(1)$  can be both second or first order, depending on the path followed. In Fig. 8, the solid line  $a$  refers to a path at  $\mu_B = 0$  vs.  $\mu_I \geq 0$  where the transition to pion condensation is continuous. The behavior of the condensates relative to this path is plotted in Fig. 10. In Fig. 11 we plot the scalar and pseudoscalar condensates at  $\mu_u = 200 \text{ MeV}$  and  $T = 140 \text{ MeV}$  vs.  $\mu_d$ .

In Fig. 12 we plot the value of the critical isospin chemical potential  $\mu_I^C$  beyond which a pion condensate forms vs. temperature  $T$  at zero baryon chemical potential  $\mu_B$ . The growth of  $\mu_I^C$  is easily understood since the pion mass (which should be twice  $\mu_I^C$ ) is expected to grow near the critical temperature for chiral symmetry restoration [38]. On the other hand, no phase transition to pion condensation is expected above the cross-over temperature for chiral symmetry restoration. Thus the line of critical values ends at  $T = 174 \text{ MeV}$ .

The pion condensate is also expected to decrease for growing temperatures: in Fig. 13 we show  $\rho$  vs.  $T$  at  $\mu_B = 0$  and  $\mu_I = 200 \text{ MeV}$ . Similar behaviors are obtained for fixed values of  $\mu_B$  and  $\mu_I$ .

#### IV. CONCLUSIONS

In this paper we have continued the study of pion condensation at finite baryon and isospin density in the NJL model that we started in ref. [14] in the case of *ladder*-QCD for small isospin chemical potentials. The extension to higher isospin chemical potentials confirms the structure predicted in ref. [11], where two-flavor QCD was simulated in the context of a random matrix model. Some difference between the two analysis is present, at low temperatures, in the region of high isospin chemical potentials, at the boundary of the region where color superconductivity should take place. Actually in this region we find that pion condensation is still active, whereas in ref. [11] the authors find that the pion condensate vanishes. We have also shown the expected behavior of scalar and pion

condensates by following different paths, for growing temperatures, both in the plane of quark chemical potentials ( $\mu_u, \mu_d$ ) and in that of isospin and baryon chemical potentials ( $\mu_I, \mu_B$ ). The analysis that we have performed should also be confirmed, with only small quantitative differences, within *ladder*-QCD.

- 
- [1] M. Buballa and M. Oertel, Phys. Lett. B **457**, 261 (1999) [arXiv:hep-ph/9810529].
  - [2] P. F. Bedaque, Nucl. Phys. A **697**, 569 (2002) [arXiv:hep-ph/9910247].
  - [3] D. Toublan and J. J. M. Verbaarschot, Int. J. Mod. Phys. B **15**, 1404 (2001) [arXiv:hep-th/0001110].
  - [4] A. Steiner, M. Prakash and J. M. Lattimer, Phys. Lett. B **486**, 239 (2000) [arXiv:nucl-th/0003066].
  - [5] D. T. Son and M. A. Stephanov, Phys. Rev. Lett. **86**, 592 (2001) [arXiv:hep-ph/0005225].
  - [6] M. G. Alford, J. A. Bowers and K. Rajagopal, Phys. Rev. D **63**, 074016 (2001) [arXiv:hep-ph/0008208].
  - [7] K. Splittorff, D. T. Son and M. A. Stephanov, Phys. Rev. D **64**, 016003 (2001) [arXiv:hep-ph/0012274].
  - [8] J. B. Kogut and D. Toublan, Phys. Rev. D **64**, 034007 (2001) [arXiv:hep-ph/0103271].
  - [9] A. W. Steiner, S. Reddy and M. Prakash, Phys. Rev. D **66**, 094007 (2002) [arXiv:hep-ph/0205201].
  - [10] F. Neumann, M. Buballa and M. Oertel, Nucl. Phys. A **714**, 481 (2003) [arXiv:hep-ph/0210078].
  - [11] B. Klein, D. Toublan and J. J. M. Verbaarschot, Phys. Rev. D **68**, 014009 (2003) [arXiv:hep-ph/0301143].
  - [12] D. Toublan and J. B. Kogut, Phys. Lett. B **564**, 212 (2003) [arXiv:hep-ph/0301183].
  - [13] M. Frank, M. Buballa and M. Oertel, Phys. Lett. B **562**, 221 (2003) [arXiv:hep-ph/0303109].
  - [14] A. Barducci, G. Pettini, L. Ravagli and R. Casalbuoni, Phys. Lett. B **564**, 217 (2003) [arXiv:hep-ph/0304019].
  - [15] A. Barducci, R. Casalbuoni, S. De Curtis, R. Gatto and G. Pettini, Phys. Lett. B **231**, 463 (1989).
  - [16] A. Barducci, R. Casalbuoni, S. De Curtis, R. Gatto and G. Pettini, Phys. Rev. D **41**, 1610

- (1990).
- [17] S. P. Klevansky, Rev. Mod. Phys. **64**, 649 (1992).
  - [18] A. Barducci, R. Casalbuoni, G. Pettini and R. Gatto, Phys. Rev. D **49**, 426 (1994).
  - [19] T. Hatsuda and T. Kunihiro, Phys. Rept. **247**, 221 (1994) [arXiv:hep-ph/9401310].
  - [20] M. A. Halasz, A. D. Jackson, R. E. Shrock, M. A. Stephanov and J. J. M. Verbaarschot, Phys. Rev. D **58**, 096007 (1998) [arXiv:hep-ph/9804290].
  - [21] J. Berges and K. Rajagopal, Nucl. Phys. B **538**, 215 (1999) [arXiv:hep-ph/9804233].
  - [22] K. Rajagopal and F. Wilczek, in M. Shifman (Ed.), *At the Frontier of Physics: Handbook of QCD*, Vol. 3, World Scientific, Singapore, p. 2061, hep-ph/0011333.
  - [23] A. Jakovac, A. Patkos, Z. Szepe and P. Szepfalussy, Phys. Lett. B **582**, 179 (2004) [arXiv:hep-ph/0312088].
  - [24] J. B. Kogut and D. K. Sinclair, Phys. Rev. D **66**, 014508 (2002) [arXiv:hep-lat/0201017].
  - [25] J. B. Kogut and D. K. Sinclair, Phys. Rev. D **66**, 034505 (2002) [arXiv:hep-lat/0202028].
  - [26] S. Gupta, arXiv:hep-lat/0202005.
  - [27] P. de Forcrand and O. Philipsen, Nucl. Phys. B **642**, 290 (2002) [arXiv:hep-lat/0205016].
  - [28] D. K. Sinclair, J. B. Kogut and D. Toublan, arXiv:hep-lat/0311019.
  - [29] Z. Fodor and S. D. Katz, Phys. Lett. B **534**, 87 (2002) [arXiv:hep-lat/0104001].
  - [30] Z. Fodor and S. D. Katz, JHEP **0203**, 014 (2002) [arXiv:hep-lat/0106002].
  - [31] C. R. Allton *et al.*, Phys. Rev. D **66**, 074507 (2002) [arXiv:hep-lat/0204010].
  - [32] M. D'Elia and M. P. Lombardo, Phys. Rev. D **67**, 014505 (2003) [arXiv:hep-lat/0209146].
  - [33] Y. Nishida, arXiv:hep-ph/0312371.
  - [34] S. Hands and D. N. Walters, arXiv:hep-lat/0401018.
  - [35] M. G. Alford, K. Rajagopal and F. Wilczek, Phys. Lett. B **422**, 247 (1998) [arXiv:hep-ph/9711395].
  - [36] A. Barducci, R. Casalbuoni, S. De Curtis, D. Dominici and R. Gatto, Phys. Rev. D **38**, 238 (1988).
  - [37] M. G. Alford, J. A. Bowers, J. M. Cheyne and G. A. Cowan, Phys. Rev. D **67**, 054018 (2003) [arXiv:hep-ph/0210106].
  - [38] A. Barducci, R. Casalbuoni, S. De Curtis, R. Gatto and G. Pettini, Phys. Rev. D **46**, 2203 (1992).

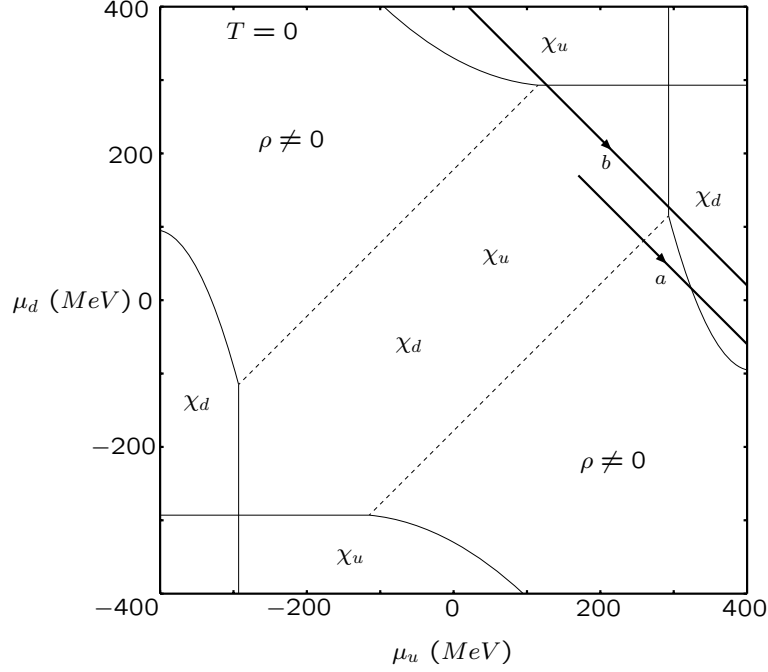


FIG. 1: Phase diagram for chiral symmetry restoration in the plane  $(\mu_u, \mu_d)$  of quark chemical potentials, at  $T = 0$ . Different regions are specified by the non vanishing of a given condensate, whereas the others are vanishing ( $\rho$ ) or order  $\sim m/\Lambda$  ( $\chi_u$  and  $\chi_d$ ). Dashed lines are for the continuous vanishing of  $\rho$  or for cross-over phase transitions for  $\chi_u$  or  $\chi_d$ , whereas solid lines are for discontinuous behaviors. The solid lines  $a$  and  $b$  refer to specific paths at fixed values of  $\mu_B$ , with  $\mu_B = 170$  MeV (line  $a$ ) relative to Fig. 3 and  $\mu_B = 210$  MeV (line  $b$ ) relative to Fig. 4.

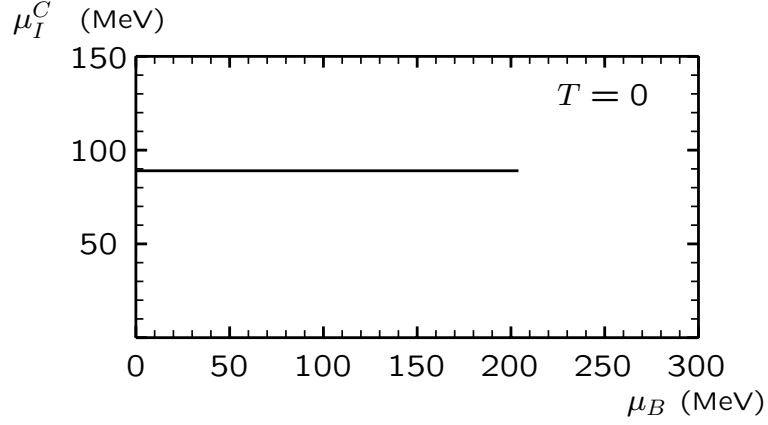


FIG. 2: Critical value of the isospin chemical potential, beyond which a pseudoscalar condensate forms, vs. baryon chemical potential, at zero temperature.  $\mu_B = 204$  MeV is the highest allowed value for pion condensation to occur. The path followed in the phase diagram of Fig. 1 is along the upper-half of the dashed line in the lower half-plane.

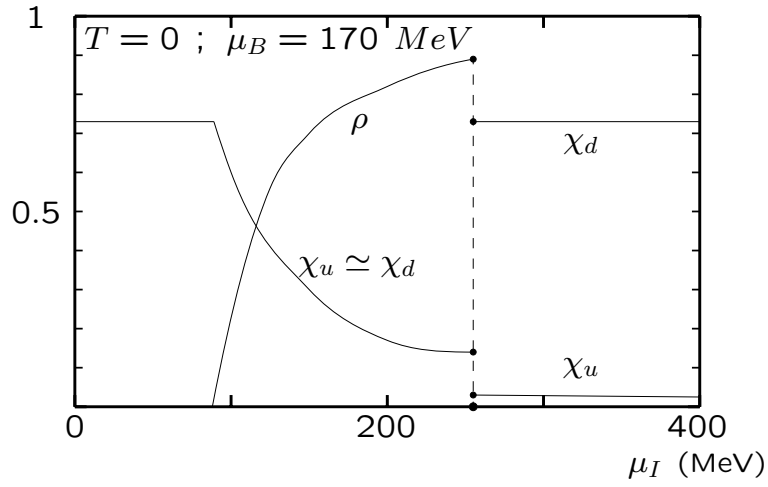


FIG. 3: Scalar and pseudoscalar condensates vs.  $\mu_I$ , for  $\mu_B = 170$  MeV and  $T = 0$ . The path followed in the phase diagram of Fig. 1 is that of the solid line a.

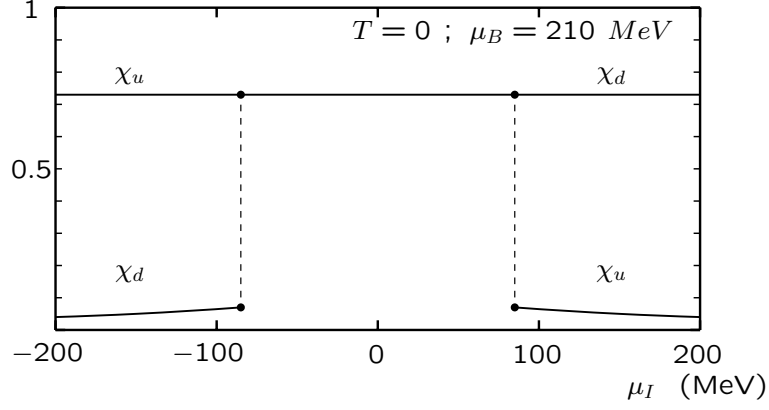


FIG. 4: *Scalar condensates vs.  $\mu_I$  for  $\mu_B = 210$  MeV and  $T = 0$ . The pseudoscalar condensate is zero. The path followed in the phase diagram of Fig. 1 is that of the solid line b.*

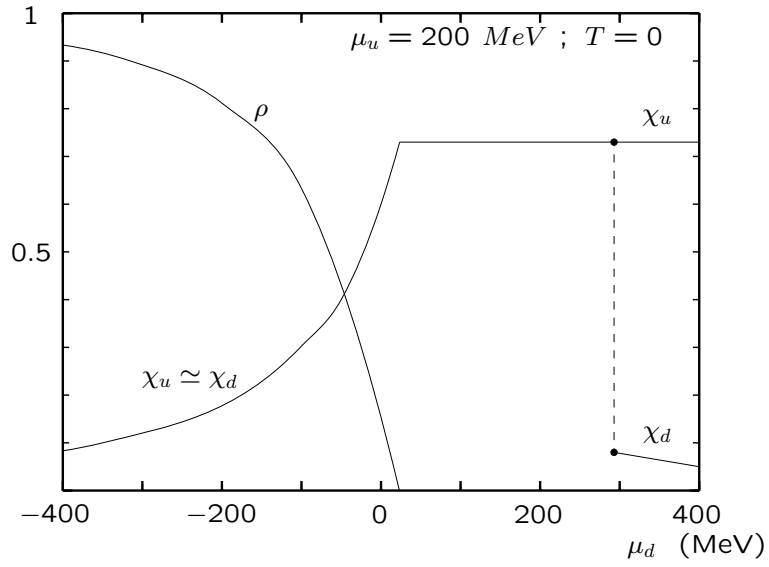


FIG. 5: *Scalar and pseudoscalar condensates vs.  $\mu_d$ , for  $\mu_u = 200$  MeV,  $T = 0$  (see Fig. 1).*

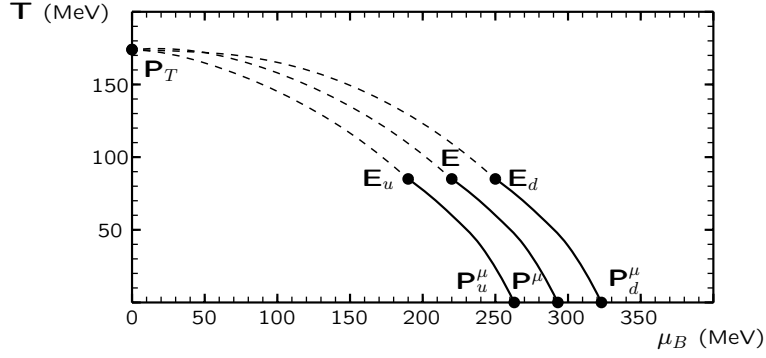


FIG. 6: Phase diagram for chiral symmetry in the  $(\mu_B, T)$  plane for zero or small isospin chemical potential  $\mu_I$ . For  $\mu_I = 0$  (central line), the cross-over transition line starts from the point  $P_T = (0, 174)$  and ends at the point  $E = (220, 85)$ . The line between  $E$  and the point  $P^\mu = (293, 0)$  is the line for the first order transition with discontinuities in the  $\langle \bar{u}u \rangle$  and  $\langle \bar{d}d \rangle$  condensates. For  $\mu_I = 30$  MeV (side lines), the two cross-over transition lines start from the point  $P_T = (0, 174)$  and end at the points  $E_u = (190, 85)$  and  $E_d = (250, 85)$ . The lines between  $E_u$  and the point  $P_u^\mu = (263, 0)$  and between  $E_d$  and the point  $P_d^\mu = (323, 0)$  are the lines for the first order transitions with discontinuities in the  $\langle \bar{u}u \rangle$  and  $\langle \bar{d}d \rangle$  condensates respectively.



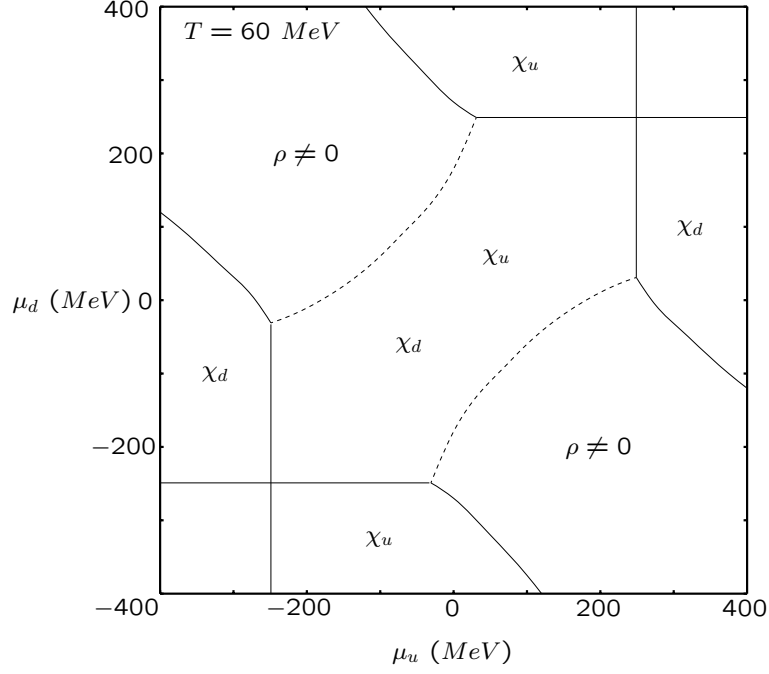


FIG. 7: Phase diagram for chiral symmetry restoration in the plane  $(\mu_u, \mu_d)$  of quark chemical potentials, at  $T = 60 \text{ MeV}$ , which is below the temperature of the critical ending point (see Fig. 6). Different regions are specified by the non vanishing of a given condensate, whereas the others are vanishing ( $\rho$ ) or  $\sim m/\Lambda$  ( $\chi_u$  and  $\chi_d$ ). Dashed lines are lines for the continuous vanishing of  $\rho$  or for cross-over phase transitions for  $\chi_u$  or  $\chi_d$ , whereas solid lines are for discontinuous behaviors.

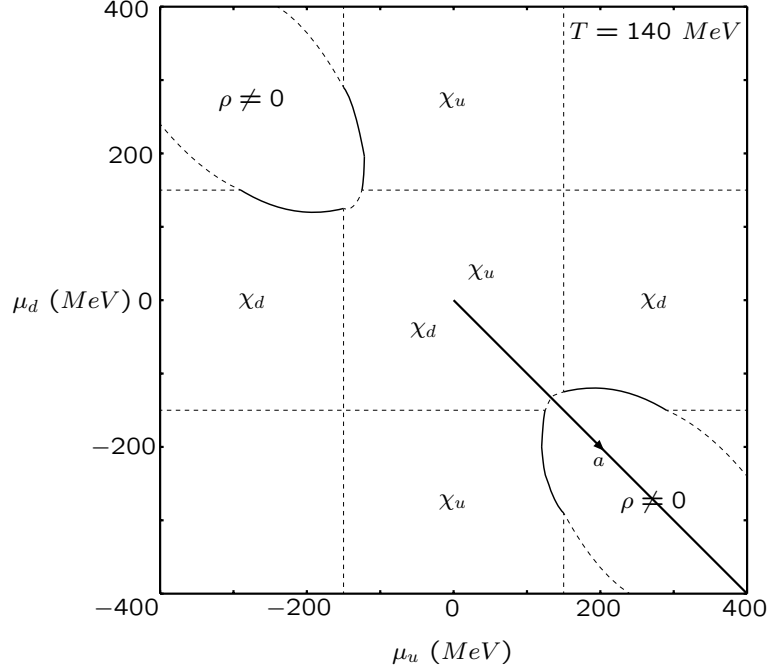


FIG. 8: Phase diagram for chiral symmetry restoration in the plane  $(\mu_u, \mu_d)$  of quark chemical potentials, at  $T = 140 \text{ MeV}$ , which is above the temperature of the critical ending point (see Fig. 6). Different regions are specified by the non vanishing of a given condensate, whereas the others are vanishing ( $\rho$ ) or  $\sim m/\Lambda$  ( $\chi_u$  and  $\chi_d$ ). Dashed lines are lines for the continuous vanishing of  $\rho$  or for cross-over phase transitions for  $\chi_u$  or  $\chi_d$ , whereas solid lines are for discontinuous behaviors. The solid line a refer to the path at  $\mu_B = 0$  vs.  $\mu_I \geq 0$  followed in Fig. 10.

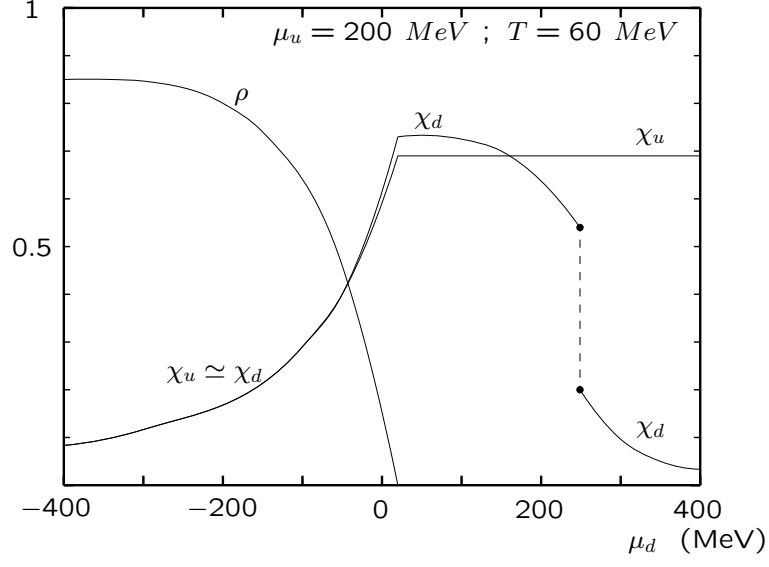


FIG. 9: *Scalar and pseudoscalar condensates vs.  $\mu_d$ , for  $\mu_u = 200$  MeV,  $T = 60$  MeV (see Fig. 7).*

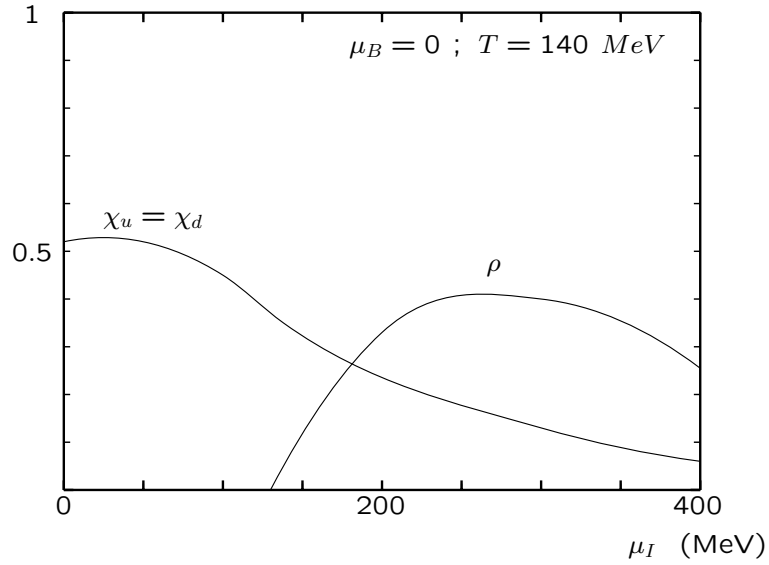


FIG. 10: *Scalar and pseudoscalar condensates vs.  $\mu_I$ , for  $\mu_B = 0$  and  $T = 140$  MeV. The figure is obtained following the path a in the phase diagram of Fig. 8.*

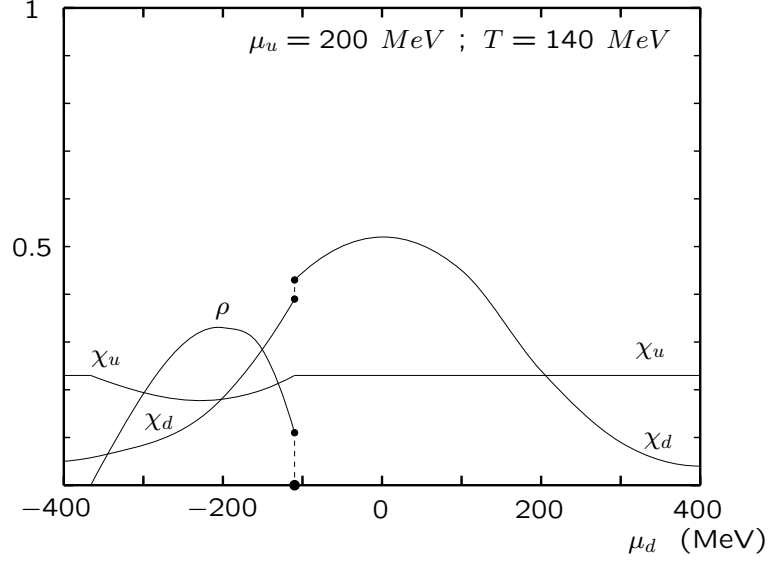


FIG. 11: *Scalar and pseudoscalar condensates vs.  $\mu_d$ , for  $\mu_u = 200$  MeV,  $T = 140$  MeV (see Fig. 8).*

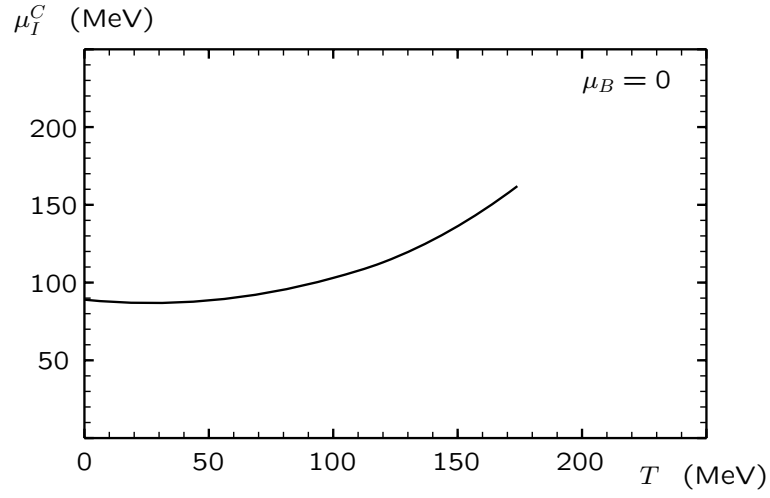


FIG. 12: *Critical value of the isospin chemical potential, beyond which a pseudoscalar condensate forms, vs. temperature, at zero baryon chemical potential.*

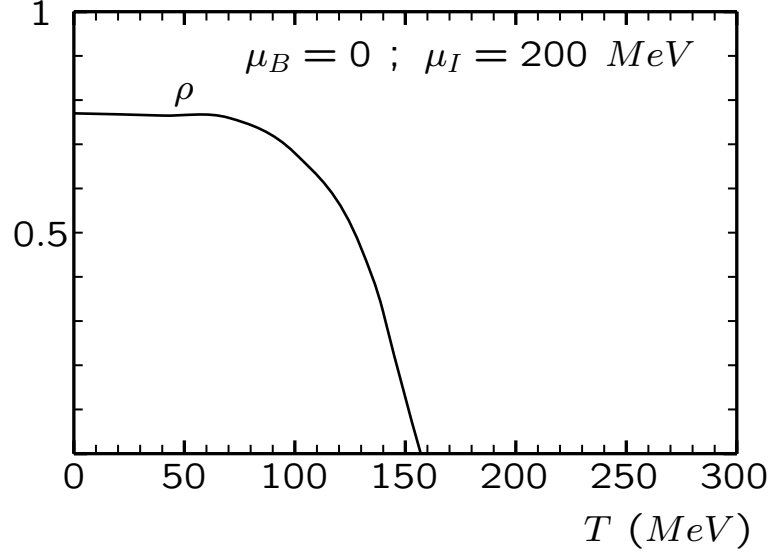


FIG. 13: *Pion condensates vs.  $T$ , for  $\mu_B =$  and  $\mu_I = 200 \text{ MeV}$ . The scalar condensates  $\chi_u$  and  $\chi_d$  are of order  $\sim m/\Lambda$ .*